*materials*

MDPI

*Article*

# Conversion of Bivalve Shells to Monocalcium and Tricalcium Phosphates: An Approach to Recycle Seafood Wastes

**Somkiat Seesanong [1], Banjong Boonchom [2,3,*], Kittichai Chaiseeda [4,*], Wimonmat Boonmee [5] and Nongnuch Laohavisuti [6]**

[1] Department of Plant Production Technology, Faculty of Agricultural Technology, King Mongkut's Institute of Technology Ladkrabang, Bangkok 10520, Thailand; ksesomki@yahoo.com
[2] Advanced Functional Phosphate Material Research Unit, Department of Chemistry, Faculty of Science, King Mongkut's Institute of Technology Ladkrabang, Bangkok 10520, Thailand
[3] Municipal Waste and Wastewater Management Learning Center, Faculty of Science, King Mongkut's Institute of Technology Ladkrabang, Bangkok 10520, Thailand
[4] Organic Synthesis, Electrochemistry and Natural Product Research Unit (OSEN), Department of Chemistry, Faculty of Science, King Mongkut's University of Technology Thonburi, Bangkok 10140, Thailand
[5] Department of Biology, Faculty of Science, King Mongkut's Institute of Technology Ladkrabang, Bangkok 10520, Thailand; bwimonmat@gmail.com
[6] Department of Animal Production Technology and Fishery, Faculty of Agricultural Technology, King Mongkut's Institute of Technology Ladkrabang, Bangkok 10520, Thailand; nongnuch.la@kmitl.ac.th
* Correspondence: kbbanjon@gmail.com (B.B.); kittichai@gmail.com (K.C.)

check for updates

**Citation:** Seesanong, S.; Boonchom, B.; Chaiseeda, K.; Boonmee, W.; Laohavisuti, N. Conversion of Bivalve Shells to Monocalcium and Tricalcium Phosphates: An Approach to Recycle Seafood Wastes. *Materials* **2021**, *14*, 4395. https://doi.org/10.3390/ma14164395

Academic Editors: Franz-Georg Simon and Ute Kalbe

Received: 21 June 2021
Accepted: 3 August 2021
Published: 5 August 2021



**Abstract:** The search for sustainable resources remains a subject of global interest and the conversion of the abundantly available bivalve shell wastes to advanced materials is an intriguing method. By grinding, calcium carbonate ($CaCO_3$) powder was obtained from each shell of bivalves (cockle, mussel, and oyster) as revealed by FTIR and XRD results. Each individual shell powder was reacted with $H_3PO_4$ and $H_2O$ to prepare $Ca(H_2PO_4)_2{\cdot}H_2O$ giving an anorthic crystal structure. The calcination of the mixture of each shell powder and its produced $Ca(H_2PO_4)_2{\cdot}H_2O$, at 900 °C for 3 h, resulted in rhombohedral crystal β-$Ca_3(PO_4)_2$ powder. The FTIR and XRD data of the $CaCO_3$, $Ca(H_2PO_4)_2{\cdot}H_2O$, and $Ca_3(PO_4)_2$ prepared from each shell powder are quite similar, showing no impurities. The thermal behaviors of $CaCO_3$ and $Ca(H_2PO_4)_2{\cdot}H_2O$ produced from each shell were slightly different. However, particle sizes and morphologies of the same products obtained from different shells were slightly different—but those are significantly different for the kind of the obtained products. Overall, the products ($CaCO_3$, $Ca(H_2PO_4)_2{\cdot}H_2O$, and $Ca_3(PO_4)_2$) were obtained from the bivalve shell wastes by a rapidly simple, environmentally benign, and low-cost approach, which shows huge potential in many industries providing both economic and ecological benefits.

**Keywords:** calcium phosphate; calcium carbonate; recycling; environmental problems; seashell

## 1. Introduction

Seafood productions contributed importantly to require for a source of protein worldwide, but it also creates huge waste quantities of solid and liquid in the processes [1]. For mollusk, shell wastes of over 13 million tons were manufactured yearly [2,3]. Three major types of mollusk informed by the Food and Agriculture Organization of the United Nations (FAO) Fisheries and Aquaculture Department are cockles, mussels, and oysters, which are consumed very largely around the world [1]. The main sources are generally from aquaculture upward than wild fisheries, amongst which oysters were dominant followed by mussels and cockles. In 2018, 5.8, 1.6, and 0.4 million tons of oyster, mussel, and cockle were produced, respectively [2]. Generally, bivalve shell wastes account for about 65–80% of live weight, which is expected to be over 5 million tons a year [4]. Large numbers of bivalve shells are dumped into public waters and/or landfills and create numerous environmental obstacles that contribute to pollution to coastal fisheries, public water surface, an

unpleasant smell as a consequence of the decomposition of organics attached to the shells, and natural landscape affecting to health/sanitation problems [2–5]. Consequently, the disposal of bivalve shell wastes is getting an extremely fatal issue for the marine aquaculture industries and various consumer countries. The increasing knowledge of sustainable evolution and research attention in innovative technologies on the conversion of bivalve shell wastes into helpful and expensive chemicals and compounds have been starting in the 21st century [4]. So far, many researchers have studied on characterizations of bivalve (cockles, mussels, and oysters) shells and reported that chemical contents consist of primarily calcium carbonate (>95%) with various crystal phases [4]. Based on their environment, the different species of shells may comprise various quantities of cation contaminations such as silicon, magnesium, aluminum, strontium, phosphorus, sodium, or sulfur [6–8].

Calcium carbonate ($CaCO_3$) naturally occurs in rocks and shells of various organisms and is widely used in construction, papermaking, pharmaceuticals, agriculture, etc. This $CaCO_3$ compound occurs naturally in three polymorphs including calcite (β), aragonite (γ), and vaterite (μ) [6–8]. Nowadays, the principal calcium carbonate production is from mineral resources, which have the risk of heavy metal contamination and are non-renewable resources, unlike calcium carbonate from bio-derived shells which are generally abundant, renewable, inexpensive, and environmentally friendly [1,4]. Based on the above mentioned, recycling seashell wastes to $CaCO_3$ raw material offers many advantages and has potential application in various fields (Figure 1). Various worldwide research shows immense potential for applications of seashells. Recently, they have been used to produce hydroxyapatite [7], nano-hydroxyapatite (nHA) [8], apatite nanoparticles [9], calcite lime [10], CaO [11,12], bio-filler in polypropylene [13], matte glaze [14], cement clinker [15], cementitious construction materials [16], expansive additive in cement mortar [17], adsorbent for Pb(II) adsorption [18], adsorbent for sulfate and metals removal [19], covalently functionalized biogenic $CaCO_3$ [20], calcined mussel shell powder (CMSP) for antistatic oil-removal [21]. However, in Southeast Asia, especially Thailand, a country with the highest bivalve (cockles, mussels, and oysters) production, the waste shell recycling means is not created appropriately, and these wastes are mainly dumped in the near areas affecting an environmental issue [22,23]. Alarmed with the problems, the Ministry of Higher Education, Science, Research, and Innovation of Thailand planned to resolve according to the Bio-Circular-Green Economy (BCG) model and financed a program to set new strategies for recycling these wastes, including establishing factories for producing calcium compounds to increase the recycling quantity of bivalve shell wastes. However, only 30% of bivalve shell wastes are reused/recycled by these factories [24,25].


**Figure 1.** Potential applications of bivalve shell wastes.

Realizing this problem, our research focuses on the conversion of bivalve shells to calcium phosphates, which are used as nutritional supplements, catalysts for some chemical reactions, fertilizers, and animal feed minerals, the mineral basis of the tooth and bone tissues, as well as for creating materials with unique properties [1,4–9]. In Thailand, monocalcium phosphate (MCP) and tricalcium phosphate (TCP) are enormously used in many fields and both compounds are imported every year. MCP has been used in huge quantities in agriculture. It is called superphosphate fertilizer, classified by three levels of $\%P_2O_5$ (single (9–20%), double (20–48%), and triple (48–58%) superphosphates), and P-21 for animal feed minerals [24,25]. Additionally, MCP is also used in large amounts in the food industry as a buffer, hardener, leavening reagent, yeast food, beverage, bakery, and nutrient [26]. TCP is widely used in huge amounts in the medical and pharmaceutical industries as medicine, tooth, bone, calcium supplement, in the animal feed industry as calcium additive and supplement, and in the food industry as various functions (acidity regulator, anticaking, emulsifying, firming, flouring, humectant, raising, stabilizer, and thickener) in many food substances under the number 341(iii) [27]. Both compounds have been synthesized to produce high-purity grades from various calcium compounds (chloride, carbonate, oxide, nitrate, acetate, etc.) and various phosphorus compounds (phosphoric acid, sodium, potassium, ammonium, etc.) by many methods including chemical precipitation [24], hydrothermal synthesis [28,29], microwave-assisted methods [30,31], precipitation of emulsions [32], sol-gel [33], crystallization of solutions [34], chemical deposition [35], electrodeposition [36], and mechanic-chemical synthesis [37]. The method performed in an individual event depends on the requisite kind of morphology, structure, and chemical content. However, the typical drawback of these synthesized methods is expensive raw materials resulting in the high cost of the obtained products which are not suitable to use for some applications such as fertilizer and animal feed industries.

Therefore, one of the solving keys for the mention-above points is to apply/recycle the bivalve shell wastes in such a route that it can be more valuable and resourcefully used to create these calcium phosphates which may solve some financial issues to purchase expensive compounds for many industries in Thailand. Although, MCP and TCP have been reportedly prepared from bivalve shell wastes such as oyster shells [38], and Mediterranean mussel shells [39], the methods used complex and high-cost processes which many parameters must be carefully controlled (concentration, pH, time, and temperature). The aim of this present work is to easily and quickly obtain calcium carbonate from bivalve shell wastes (cockles, mussels, oysters) and then subsequently use it to produce MCP and TCP by using an easy, cost-effective, and environmentally benign method. Moreover, this work also highlights some potential applications for shell wastes that can bring both economic and ecological benefits.

## 2. Materials and Methods

### *2.1. Starting Reagents*

Raw reagents utilized for the current study were waste bivalve shells of cockle, mussel, and oyster collected from seafood restaurants of fishermen residing in areas of the Chonburi beaches in eastern Thailand. The individual kind of seashells derived in the primitive shape was carefully cleaned with triply distilled water and dried in an oven at 100 °C for 3 h. Each kind of dried seashell was pulverized to produce fine powder by using an agate mortar and pestle and then was sieved in 100 mesh (150 μm). All fine seashell powders were then characterized to identify the purity and solid phase of calcium carbonate before proceeding to the preparation of the calcium phosphates. Fine seashell powders of cockle, mussel, and oyster were $CaCO_3$ compounds and denoted with the sample codes CSP, MSP, and OSP, respectively.

### *2.2. Monocalcium Phosphate Monohydrate ($Ca(H_2PO_4)_2{\cdot}H_2O$, MCPM) Preparation*

A collection of monocalcium phosphate hydrate samples was synthesized by the reaction of individual seashell powder (cockle (CSP), mussel (MSP), and oyster (OSP)

shells) with 85 wt% phosphoric acid and distilled water, using a constant-addition method modified from the generic reaction reported in previous work [10].

Briefly, 15 mL of 85 wt% $H_3PO_4$ was slowly added into a beaker (100 mL), which contains 9 g of CSP, and was constantly stirred with a Teflon stir bar. This mixing reaction exhibited an exothermic process noticed by increasing temperature (65 °C). Then, 12 mL of distilled water ($H_2O$) was immediately added into the resulting mixture with constant stirring until $CO_2$ gas bubbles are no evolved (about 30 min). The resulting reaction has been stayed in the open air for about 3 h to become dried powder of monocalcium phosphate hydrate without other processes such as filtration and drying with temperature control. The monocalcium phosphate hydrate obtained from CSP was labeled with the sample code MCP-C. For MSP and OSP, the processes were repeated in the same way as CSP, and the obtained products were labeled as MCP-M and MCP-O, respectively.

### *2.3. Tricalcium Phosphate Anhydrous ($Ca_3(PO_4)_2$, TCP) Preparation*

A series of tricalcium phosphate samples was prepared by mixing powders of individual seashell powder (cockle (CSP), mussel (MSP), and oyster (OSP) shells) with their prepared monocalcium phosphate hydrate pair (MCP-C, MCP-M, and MCP-O). The generic reaction is:

$$2CaCO_3(s) + Ca(H_2PO_4)_2{\cdot}H_2O(s) \rightarrow Ca_3(PO_3)_2(s) + H_2O(g) \quad (1)$$

In the typical way, 2.0 g of CSP and 2.52 g of MCP-C were weighed and then well mixing by grinding in a crucible. Then, the mixed powder was calcined at 900 °C for 3 h in a furnace. Its final product after heating is tricalcium phosphate, labeled as TCP-C. The tricalcium phosphate powders prepared from the mixed powders of MSP + MCP-M and OSP + MCP-O were prepared in the same way as CSP + MCP-C and the obtained products were labeled as TCP-M and TCP-O, respectively.

### *2.4. Sample Characterization*

#### 2.4.1. Thermogravimetric Analysis (TA)

The thermal behaviors of the dried fine seashell powders and monocalcium phosphate monohydrate were analyzed by a thermogravimetric/differential thermal analyzer (TG-DTA, Pyris Diamond, Perkin Elmer). The experiments were performed in the static air, at the heating rates of 10 °C $min^{-1}$ over the temperature range from 30 to 900 °C and the $O_2$ flow rate of 100 mL $min^{-1}$. The sample mass of about 6.0–10.0 mg was filled into an alumina crucible without pressing. The thermogram of a sample was recorded in an open aluminum pan using $Al_2O_3$ as the reference material.

#### 2.4.2. Fourier Transform Infrared (FTIR) Spectroscopy

The molecular structures were measured by a Fourier Transform Infrared Spectrophotometer (FTIR, Spectrum GX, Perkin Elmer), which were recorded in the range of 4000–400 $cm^{-1}$ with eight scans and the resolution of 4 $cm^{-1}$ using KBr pellets (spectroscopy grade, Merck).

#### 2.4.3. Powder X-ray Diffraction (XRD)

The structure of the prepared samples was recorded by X-ray powder diffraction using an X-ray diffractometer (D8 Advance, Bruker AXS GmbH) with Cu K radiation ($\lambda$ = 0.1546 nm) operating at the condition of 40 kV and 40 mA. The specimen was pulverized into a fine powder and used for the analysis. The diffraction angle was continuously scanned from 10° to 60° in 2$\theta$ at a scanning rate of 2°/min. A range of 10–60° is shown in the figures because no relevant peaks occurred in the excluded region.

#### 2.4.4. Scanning Electron Microscopy (SEM)

The morphology of the selected resulting samples was determined by a scanning electron microscope using LEO SEM VP1450 after gold coating.

## 3. Results and Discussion

### *3.1. Characterization Results of Bivalve Shell Powders*

Figure 2 displays TG/DTG curves of the CSP, MSP, and OSP samples, which are quite similar. TG lines of each sample show the mass loss in the region of 600–800 °C, which correspond to a strong single peak of DTG curves at 752, 772, 750 °C for the CSP, MSP, and OSP samples, respectively. Four DTG peaks observed at 515, 540, 569, and 625 °C for the MSP sample may have resulted from other cation contaminations that may be formed the mixing phase of metal carbonates, which can be not pointed out still clearly. The quantities of mass loss are found to be 43.1% for the CSP sample, 43.9% for the OSP sample, and 48.4% for the MSP sample. The thermal results were well consistent with those of the reference data of $CaCO_3$ and theoretical data [17,40,41]. The thermal behavior obtained indicates that the bivalve shell powders can be transformed to CaO by calcination at above 772 °C, which may be useful for the production of this compound to be used in specific applications.

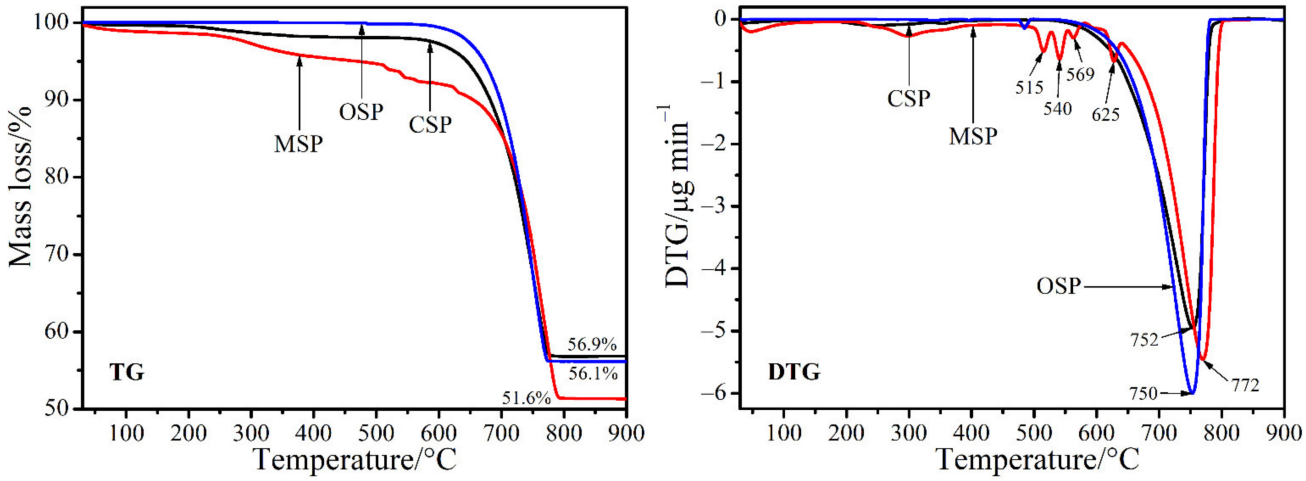


**Figure 2.** TG and DTG curves of the bivalve shell (CSP, MSP and OSP) powders.

Figure 3 illustrates FTIR spectra of the CSP, MSP, and OSP samples that are quite similar due to fundamental vibrational bands of $CO_3^{2-}$ block unit in the $CaCO_3$ structure for each sample. The vibrational modes of the $CO_3^{2-}$ anion are divided into three types [42]: (i) internal vibrational modes of ($CO_3^{2-}$) groups, (ii) hydroxyl vibrations (in the case of hydroxyl carbonates ≈ 900 cm$^{-1}$, 1500–1600 cm$^{-1}$, and 3400 cm$^{-1}$), and (iii) vibrational M-O modes from the interactions between the cation and oxygen of either ($CO_3^{2-}$) or $OH^-$ (external or lattice modes). The carbonate anion ($CO_3^{2-}$) is a nonlinear structure with four atoms resulting in six ($3 \times 4 - 6$) normal modes of vibrations [43]. The six normal vibrational modes are a nondegenerate symmetric stretch ($v_1$; A′$_1$: Raman active), nondegenerate asymmetric (out of plane) bend ($v_2$; A″$_1$: IR active), doubly degenerate asymmetric stretch ($v_3$; E′: Raman and IR active), and doubly degenerate symmetric (in-plane) bend ($v_4$; E′: Raman and IR active). The FTIR spectra of the CSP, MSP, and OSP samples were analyzed according to this theory. Two strong intense bands at 696 cm$^{-1}$ and 863 cm$^{-1}$ are assigned to the $\nu_4$ and $\nu_2$ modes, respectively. A weak band at 1030 cm$^{-1}$ is contributed to $v_1$ mode. A band at 1413 cm$^{-1}$, looking like a mountain, is related to $v_3$ mode. A weak band observed at 1782 cm$^{-1}$ may be respected as the combination bands of $\nu_4 + \nu_1$ modes. A weak band at 2520 cm$^{-1}$ and a broad band around 2875 cm$^{-1}$ may be regarded as a combination of or/and overtone of $\nu_4$, $\nu_3$, and $\nu_1$ modes. A single band at 3453 cm$^{-1}$ was assigned to the OH-stretching modes. For the FTIR results of all bivalve shells, the $v_1$ mode that appear normally active in Raman is observed and $v_3$ and $v_4$ modes are not shown doubly degenerate bands, which may be correlated with the atomic cation masses and the presence of molecules belonging to site symmetry of their structures [44]. The FTIR results obtained are very similar to that of the calcite phase of

$CaCO_3$ in literature [43,44], which indicates that the CSP, MSP, and OSP samples have the main content as this crystalline phase.

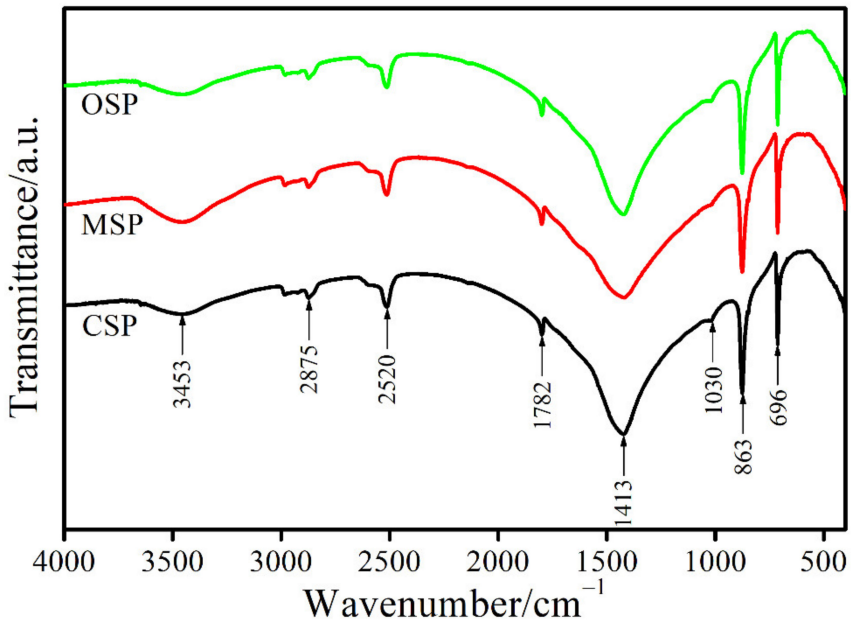


**Figure 3.** FTIR spectra of the bivalve shell (CSP, MSP and OSP) powders.

XRD patterns of the CSP, MSP, and OSP samples are very similar and are exhibited in Figure 4. Bivalve (cockle, mussel, and oyster) shells, biological wastes are primarily made up of calcium carbonate (≥96wt%) and little contaminations of other chemical contents. It can clearly indicate that the main crystalline phases of the CSP, MSP, and OSP samples are calcite (β-$CaCO_3$) and minor aragonite are detected for OSP while little vaterite is detected for the other two samples, shown in Figure 4. The diffraction intensity is the calcite (002) 2θ = 29.81 and the next to strongest are the calcites at (111), (012), (202), (112) (200), and (202), respectively. The XRD analysis verified that the crystalline phase of $CaCO_3$ in the CSP, MSP, and OSP samples was calcitic polycrystals, which was found to match with the PDF data file of $CaCO_3$ (PDF no.72–1937) [41,45]. The XRD results are in well agreement with the FTIR data.

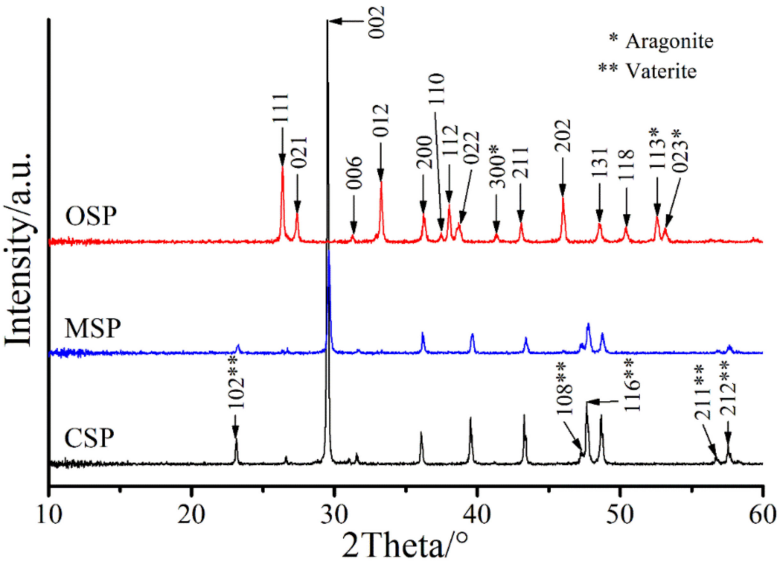


**Figure 4.** XRD patterns of the bivalve shell (CSP, MSP and OSP) powders.

SEM micrographs of the CSP, MSP, and OSP samples exhibit different morphological features and are shown in Figure 5. SEM image of CSP reveals an elongated, partly polyhedral morphology of rod-like crystals (up to 10 μm long) with different sizes and forms. SEM image of MSP reveals elongated, partly polyhedral morphology of sheet-like crystals with different sizes (5–10 μm). Finally, the SEM image of OSP reveals plate-like crystals of different sizes, which are agglomerated.

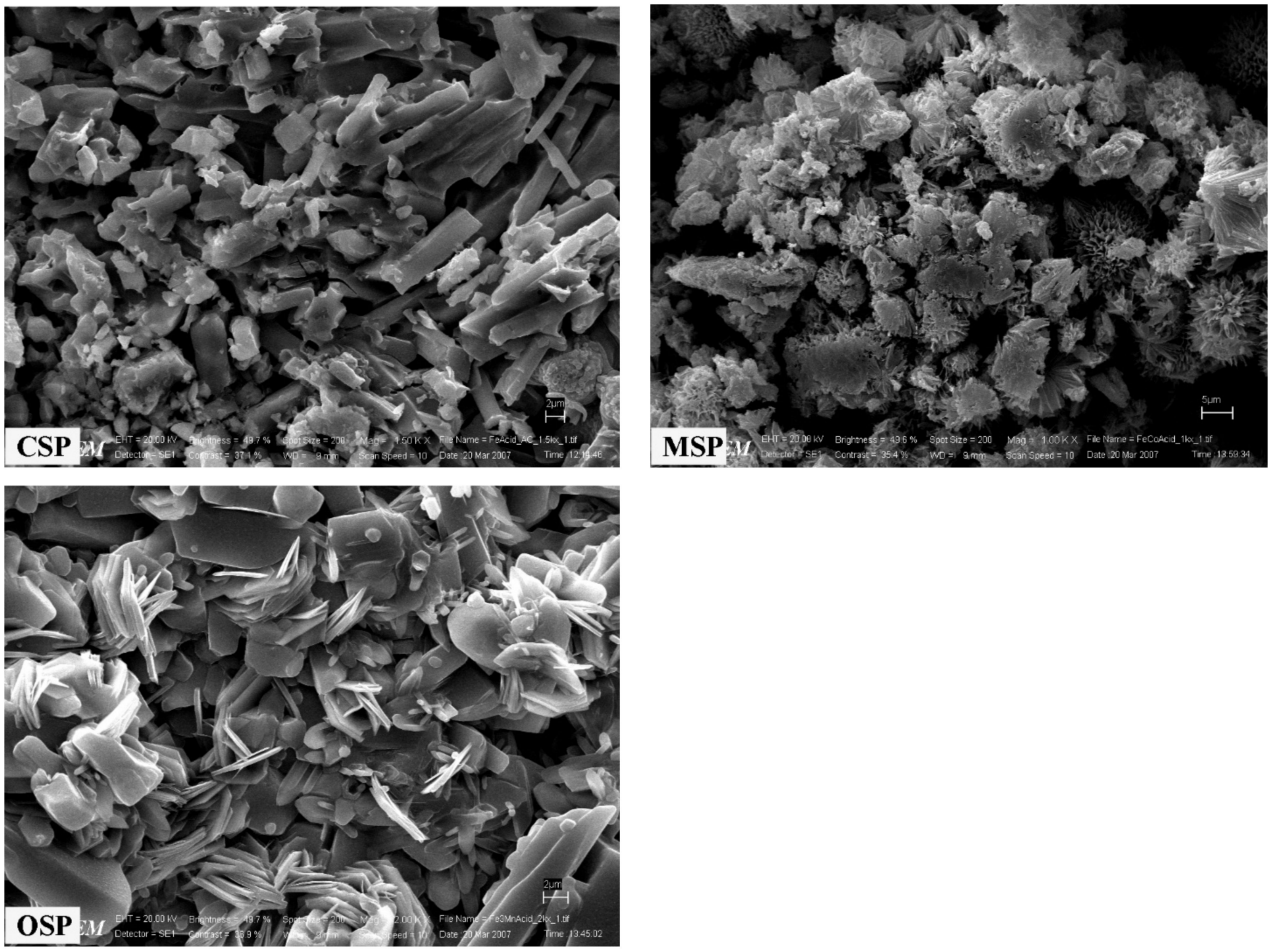


**Figure 5.** SEM micrographs of the bivalve shell (CSP, MSP and OSP) powders.

### *3.2. Characterization Results of Monocalcium Phosphates*

TG/DTG curves of three monocalcium phosphate samples prepared from cockle (CSP), mussel (MSP), and oyster (OSP) shell powders, labeled as MCP-C, MCP-M, and MCP-O, respectively, are displayed in Figure 6. TG lines of all samples showing the mass loss in the range of 100–600 °C are similar. The mass losses found to be around 20% for each sample correspond to the loss of three water molecules in structure. Total mass losses found to be 18.9% for MCP-C, 25.0% for MCP-M and 17.3% for MCP-O are slightly different from that of theoretical value at 21.4% [41,46]. The obtained results indicate that the number of water molecules in $Ca(H_2PO_4)_2 \cdot nH_2O$ structure would be 0.7, 1.5, and 0.4 mole for the MCP-C, MCP-M, and MCP-O samples, respectively. The number of crystal water found in the range of 0-n < 2 is an impossible theory, which is consistent with that of the previous works [24,26,41,46]. The relative with TG data, DTG curves of the MCP-C, MCP-M, and MCP-O samples showing the numbers and peak positions of steps of thermal transformation are different. Four DTG peaks are observed at 127, 178, 224, and 330 °C for the MCP-C sample and 127, 185, 245, and 330 °C for the MCP-M sample while five DTG peaks occur at 127, 185, 224, 265, and 330 °C for the MCP-O sample. Two peaks

that occurred below 200 °C correspond to the dehydration steps of about one molecule of water. Two/three peaks observed in the range of 200–330 °C relate to deprotonated steps of two dihydrogen phosphate ($H_2PO_4^-$) anions. General mechanism reactions of thermal transformation could be:

$$Ca(H_2PO_4)_2{\cdot}H_2O(s) \overset{\text{below}200^\circ C}{\rightarrow} Ca(H_2PO_4)_2(s) + H_2O(g) \quad (2)$$

$$Ca(H_2PO_4)_2(s) \overset{200-330^\circ C}{\rightarrow} Ca_3(PO_3)_2(s) + 2H_2O(g) \quad (3)$$

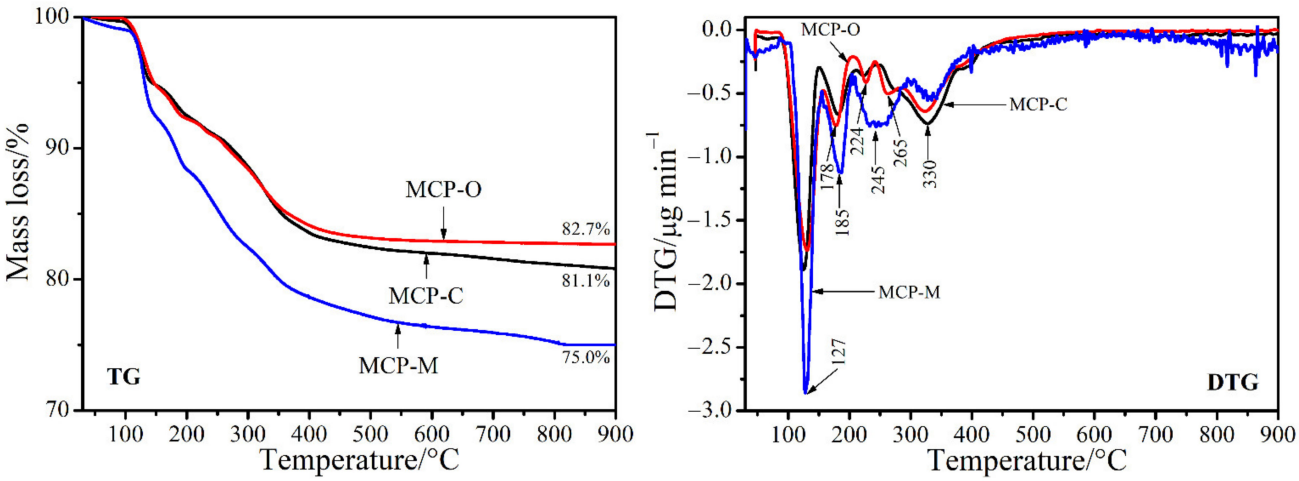


**Figure 6.** TG and DTG curves of MCP-C, MCP-M, and MCP-O samples.

The final decomposition of $Ca(H_2PO_4)_2{\cdot}H_2O$ to calcium polyphosphate $Ca_3(PO_3)_2$, as revealed by reaction (3), occurred at above 400 °C. Many peaks in DTG curves observed for three $Ca(H_2PO_4)_2{\cdot}H_2O$ samples may indicate the splitting of each step of the dehydration step (reaction 2) and deprotonated hydrogen phosphate reaction (reaction 3). This result could be regarded to be affected by different inter/intramolecular interactions due to the different surroundings of water and $H_2PO_4^-$ within the structure. Thermal properties of $Ca(H_2PO_4)_2{\cdot}H_2O$ prepared from different bivalve shells giving the different results indicate clearly that this property is dependent on raw materials.

Figure 7 presents FTIR spectra of the MCP-C, MCP-M, and MCP-O samples that are very similar because of fundamental vibrational bands of $H_2PO_4^-$ and $H_2O$ block units in the $Ca(H_2PO_4)_2{\cdot}H_2O$ structure for each sample. The vibrational modes of the $H_2PO_4^-$ anion are characterized by two types [47,48]: (i) the $PO_4^{3-}$ ($T_d$ symmetry) internal vibrations, and (ii) the vibrations involving OH motions. The dihydrogen phosphate anion ($H_2PO_4^-$) is a nonlinear structure containing seven atoms, which must have 15 ($3 \times 7 - 6$) normal vibrational modes [43]. The nine vibrations coming from the $PO_4^{3-}$ ($T_d$ symmetry) contain well-known normal modes: symmetric stretching ($\nu_1(A_1)$), symmetric bending ($\nu_2(E)$), asymmetric stretching ($\nu_3(F_2)$), and asymmetric bending ($\nu_4(F_2)$) modes. The existence of two P-OH bonds results in a decreasing molecular symmetry of the $H_2PO_4^-$ anion from its highest possible symmetry of the $C_{2v}$ point group. As a result, the degenerate modes of $\nu_2(E)$, $\nu_3(F_2)$, and $\nu_4(F_2)$ are fully lifted: $\nu_2(E)$ separates into two modes ($A_1 + A_2$) and $\nu_3(F_2)$ and $\nu_4(F_2)$ into three modes ($A_1 + B_1 + B_2$) each. These eight vibrations happen from the intra-ionic coupling interaction of two longer P- OH and two shorter P-O bonds for the $PO_4$ stretching vibrations, which may also be led to additional modes as $\nu_s(P(OH)_2)$, $\nu_{as}(P(OH)_2)$, $\nu_s(PO_2)$, and $\nu_{as}(PO_2)$ for each $H_2PO_4^-$ group. The six vibrations linking OH motions are characteristic for the $H_2PO_4^-$ anion consisting of three modes ($\nu$(OH), $\delta$(OH), and $\gamma$(OH)) for each POH group. For water molecules, fundamental vibrations contain three normal vibrations: symmetric stretching ($\nu_1$(OH)), symmetric bending($\nu_2$(HOH)), and asymmetric stretching ($\nu_3$(OH)) and three vibrations (wagging,

rocking, and twisting). The bands observed in spectra of each sample are 493, 565, 690, 862, 963, 1091, 1164, 1237, 1388, 1679, 1700, 2311, 2440, 2960, 3263, 3470 $cm^{-1}$, which are assigned to $\nu_2(PO_4^{3-})$, $\nu_4(PO_4^{3-})$, $L_1(H_2O)$, $\gamma$(OH), $\nu_{as}(P(OH)_2)$, $\nu_s(PO_2)$, $\nu_{as}(PO_2)$, $\delta$(OH) (1), $\delta$(OH) (2), $\nu_2$(HOH), $\nu$(OH) or C band, $\nu$(OH) or B band, $\nu$(OH) or B band, $\nu$(OH) or A band, ($\nu_1$(OH)) of $H_2O$, and ($\nu_3$(OH)) of $H_2O$, respectively [49]. The FTIR results obtained are very similar to that of the $Ca(H_2PO_4)_2{\cdot}H_2O$ in literature [49], which confirms that the MCP-C, MCP-M, and MCP-O samples have major content as this crystal phase.

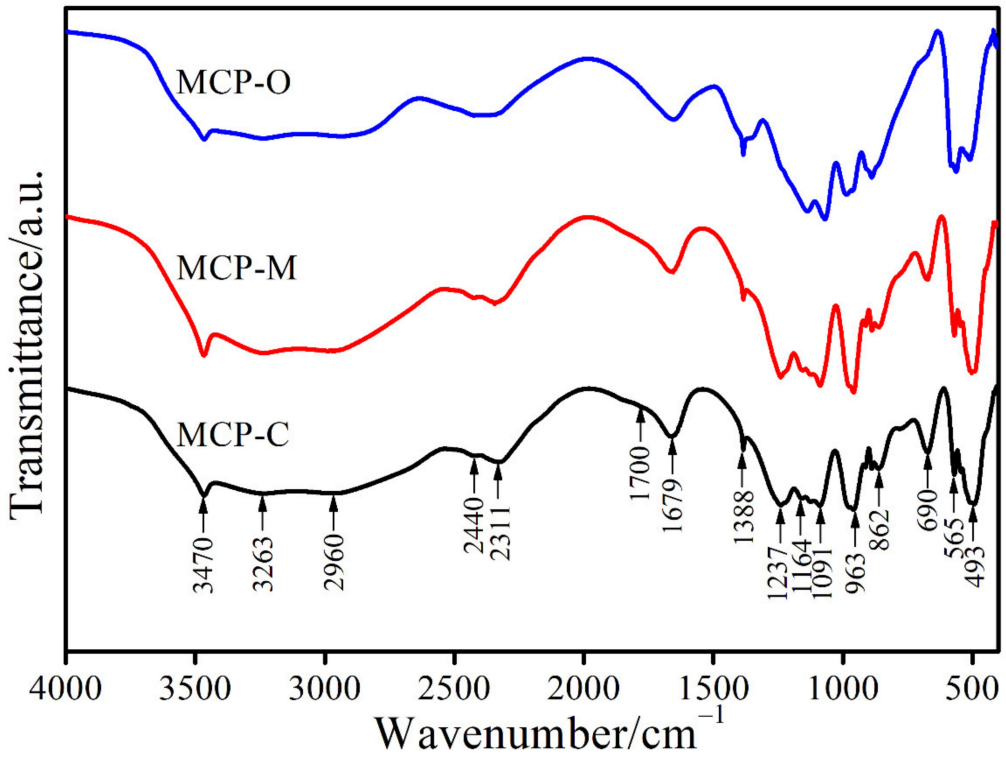


**Figure 7.** FTIR spectra of MCP-C, MCP-M, and MCP-O samples.

X-ray diffraction patterns of the MCP-C, MCP-M, and MCP-O samples (Figure 8) are the same 2θ positions but intense peaks are different. All detectable peaks of the obtained MCP-C, MCP-M, and MCP-O samples indexed as the $Ca(H_2PO_4)_2{\cdot}H_2O$ structure match with the standard data of PDF no. 70–0090 [41,46]. The XRD patterns exhibit two sharp characteristic peaks at 2θ = 22.95 and 24.18° corresponding to (0–21) and (210) reflections for anorthic crystal structure of $Ca(H_2PO_4)_2{\cdot}H_2O$. The labeled diffraction peaks can be indexed according to standard XRD data and XRD peaks of other phases were not observed, confirming the pure compounds obtained under study. The XRD results and the FTIR data are well coincident.

Figure 9 presents the typical micrographs of the three selected powder (MCP-C, MCP-M, and MCP-O) samples. As shown in Figure 9, the MCP-C particles resemble polyhedral morphologies of sheet shapes with smooth surfaces. The MCP-M particles seem to have inherited the polyhedral morphologies of the plate-like microstructures with smooth surfaces. The MCP-O particles show polyhedral morphologies of lamellar-like shapes with smooth surfaces. Morphologies of three $Ca(H_2PO_4)_2{\cdot}H_2O$ samples prepared different bivalve (cockle, mussel, and oyster) shells are slightly different in shape and particle size but these morphologies are significantly from those of raw material powders.

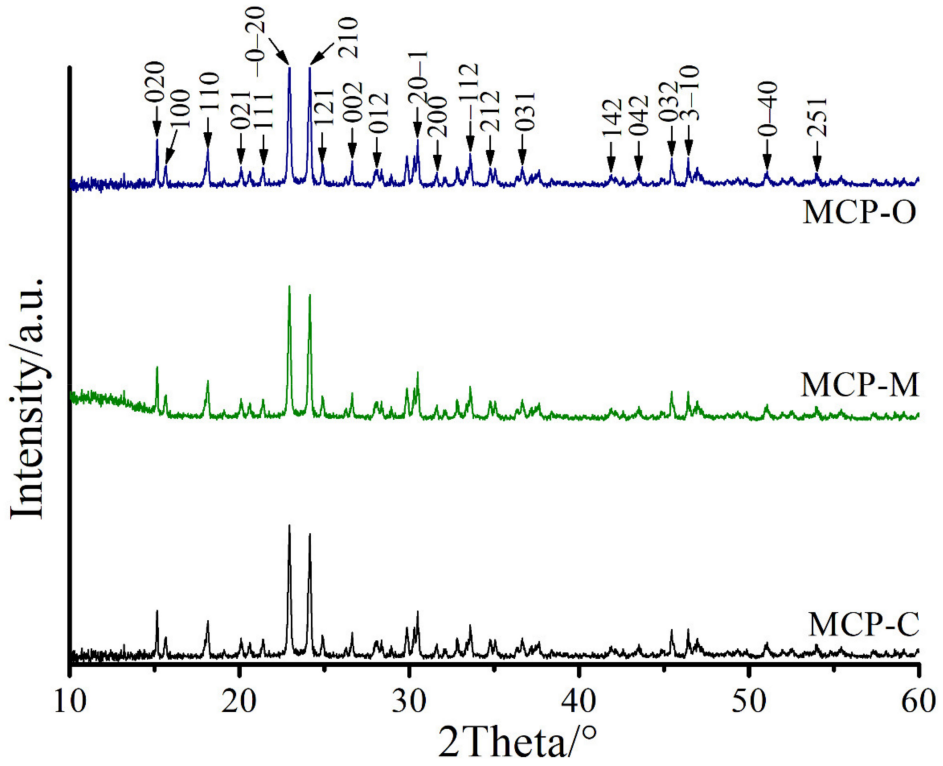


**Figure 8.** XRD patterns of MCP-C, MCP-M, and MCP-O samples.

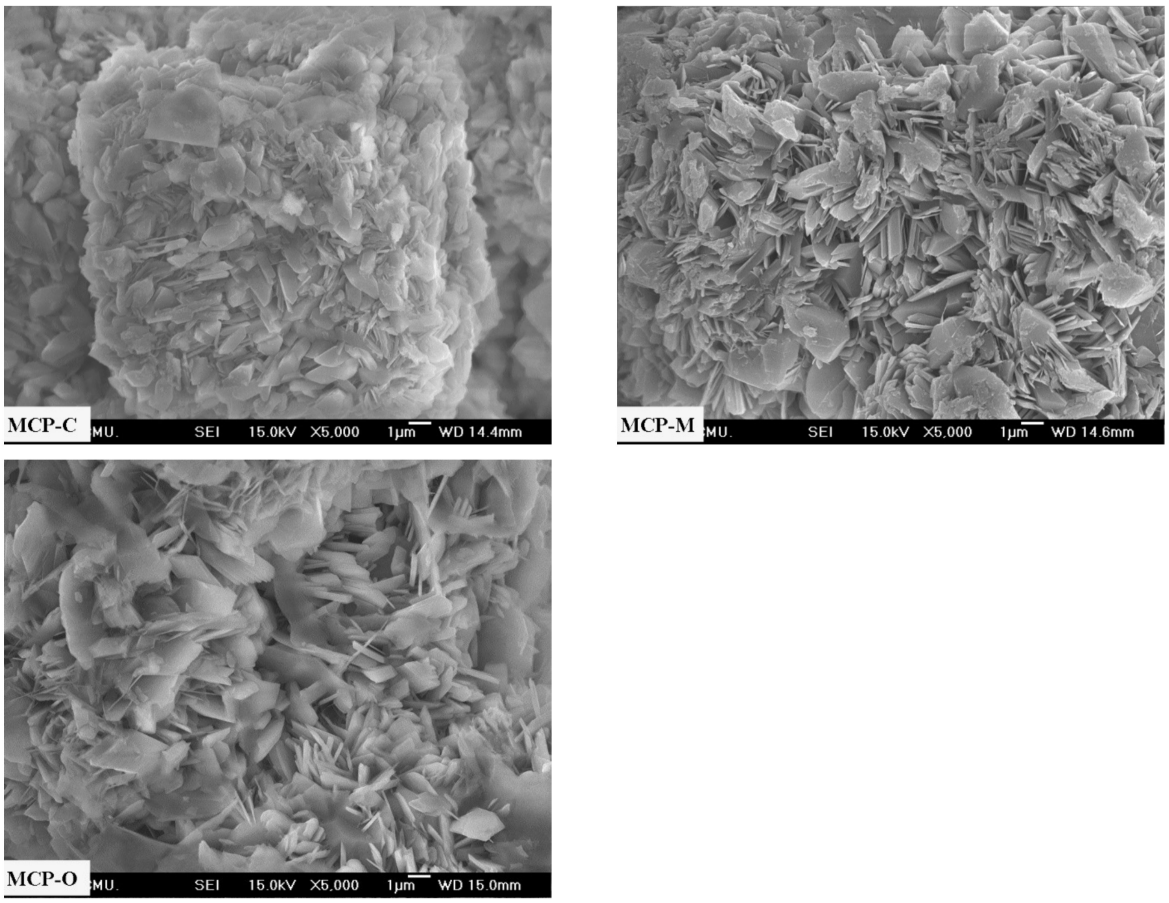


**Figure 9.** SEM micrographs of MCP-C, MCP-M and MCP-O samples.

### *3.3. Characterization Results of Tricalcium Phosphates*

For FTIR spectra of tricalcium phosphates prepared from the calcination of the mixture of the produced monocalcium phosphates with its calcium raw materials (cockle, mussel, and oyster shells), labeled as the TCP-C, TCP-M, and TCP-O and shown in Figure 10. The FTIR spectra of each sample are very similar due to the fundamental vibrating unit, $PO_4^{3-}$ anion containing within the structure. Vibrational modes are discussed similarly with the previous section and 9 ($3 \times 5 - 6$) normal vibrational modes of each phosphate group will be assigned [41]. In theory, the $\nu_3(F_2)$ and $\nu_4(F_2)$ modes are active in infrared while the $\nu_1(A_1)$ and $\nu_2(E)$ modes are active in Raman [42]. Vibrational bands of the $PO_4^{3-}$ anion for all prepared products detected in the regions of 700–450 and 1250–900 $cm^{-1}$ are defined to the $\nu_4(PO_4^{3-})$ and $\nu_3(PO_4^{3-})$ modes, respectively. Various vibrational peaks in these frequency regions insist on the presence of distinct nonequivalent phosphate block units in each structure and the loss of the degenerate modes of vibration resulting from correlation field splitting [42,43]. Additionally, a strong $\nu_s$(POP) band (721 $cm^{-1}$) occurred is known to be the most striking characteristic of polyphosphate vibration.

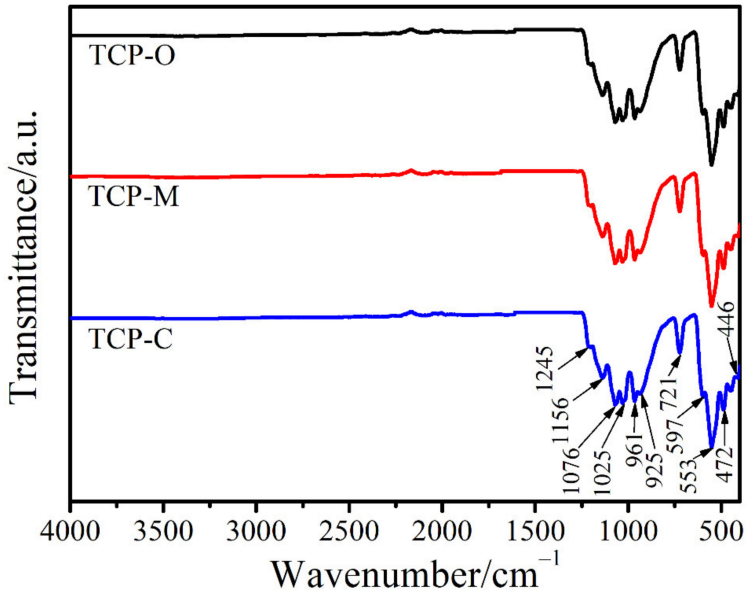


**Figure 10.** FTIR spectra of TCP-C, TCP-M and TCP-O samples.

The XRD patterns of TCP-C, TCP-M, and TCP-O samples were indexed as $Ca_3(PO_4)_2$ structures, which are classified using the standard data from the International Centre for Diffraction Data (ICDD), exhibited in Figure 11. The powders performed by different shells match with PDF no. 55–0898. In all the prepared samples, the maximum peak relating with the crystallinity of beta phase was detected at $2\theta = 31.5°$, corresponding to the (021) planes, and indicating rhombohedral crystal phase, which agrees with the previous reports [50,51]. From the XRD data of the prepared TCP samples, no other identified peaks related to impurities and any intermediate or remaining raw materials are noted, which further insists on the purity of the synthesized β-$Ca_3(PO_4)_2$ products. The obtained FTIR data of all the synthesized samples are consistent with the XRD results, which verify the classification of each compound.

The typical micrographs of the three selected powder (TCP-C, TCP-M, and TCP-O) samples are presented in Figure 12. The TCP-C particles look like the coarse surface on the grain-like shape and are highly agglomerated. The TCP-M particles were like polyhedral morphology of grain shape with uniform particles of 0.5–5.0 μm in size and agglomerations appear. The TCP-O particles were like polyhedral granular with identical particles of 0.2–5.0 μm in size and smooth surfaces. The difference of particle sizes and morphologies of three $Ca_3(PO_4)_2$ samples was caused by the different kinds of used bivalve shells as

raw reagents. The difference of particle sizes and morphologies of the three $Ca_3(PO_4)_2$ samples was caused by the different kinds of used bivalve shells as raw reagents. The SEM micrograph data of the obtained products are significantly different from those of the raw material powders.

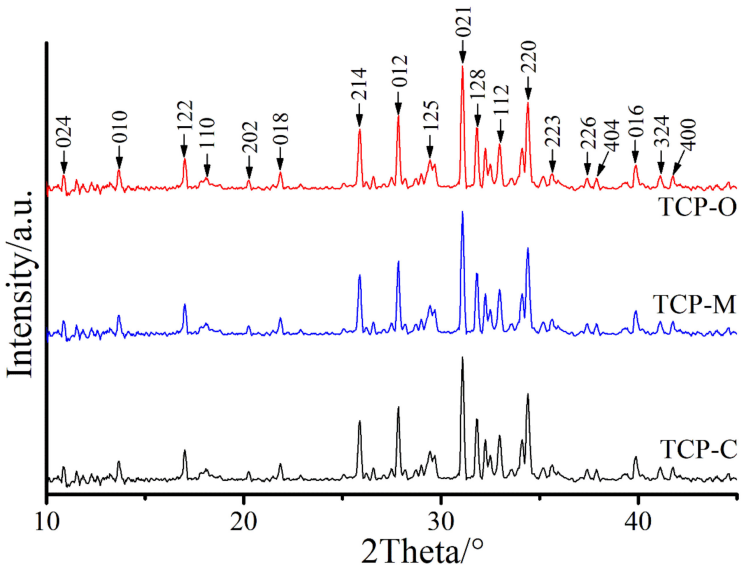


**Figure 11.** The XRD patterns of TCP-C, TCP-M, and TCP-O samples.

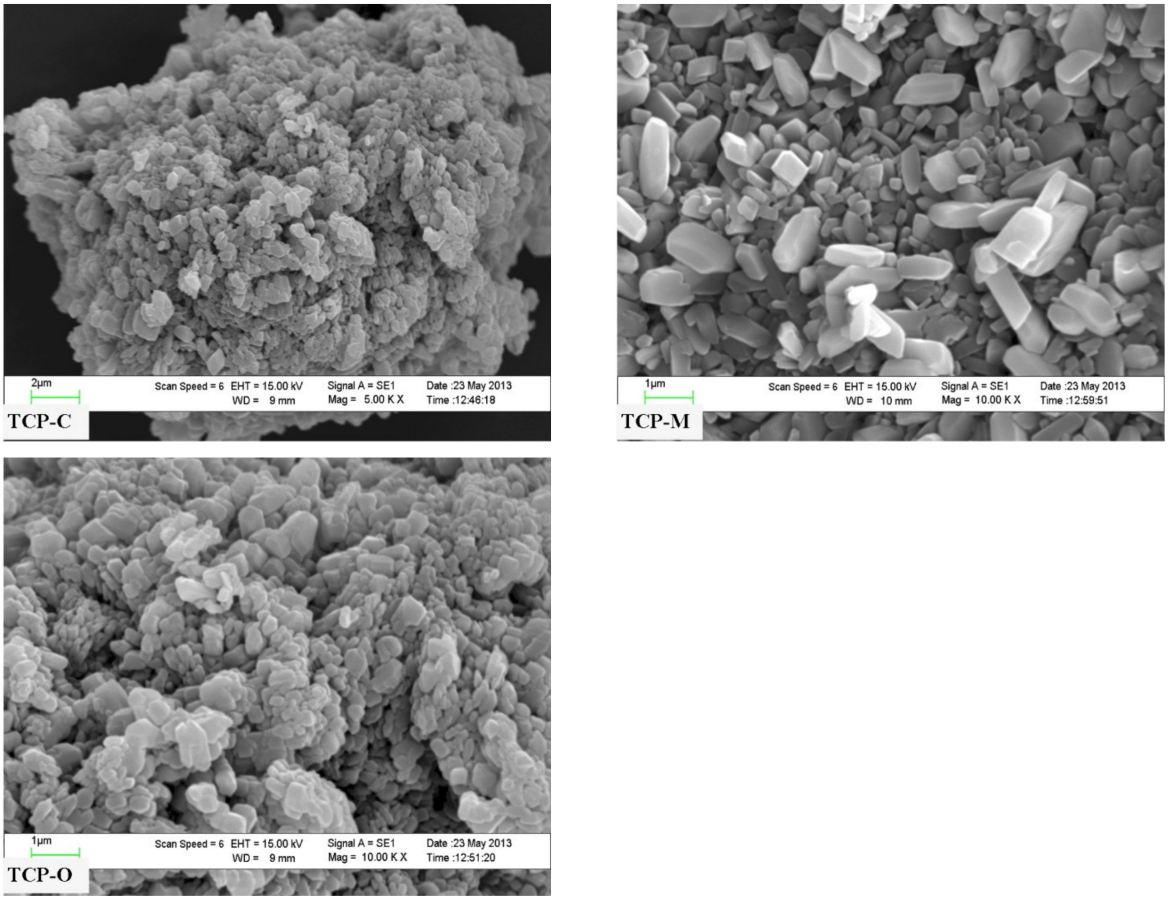


**Figure 12.** SEM micrographs of TCP-C, TCP-M and TCP-O samples.

## 4. Conclusions

With depleting natural resources, it is important to find new sustainable sources of materials and in this research, MCP and TCP were successfully produced from bivalve shells that include cockle, mussel, and oyster. In addition, by recycling these seafood wastes we also help remove large amounts of shell wastes that could pose health and environmental hazards. The method reported herein is simple, rapid, cost-effective, and environmentally friendly. MCP and TCP obtained from this method showed resemble characteristics to previous reports, indicating high purities. The slight differences in thermal properties of the $CaCO_3$ and MCP prepared depend on the starting shell powders. The morphologies of all the prepared samples were significantly different clearly indicating the raw material's effect on this property. Overall, MCP and TCP converted from these bivalve shell wastes, have a huge potential to be used in many industrials bringing about both environmental and economic benefits.

**Author Contributions:** S.S. conceived and designed the experiments; B.B. performed the experiments, analyzed the data and wrote the manuscript; K.C. contributed SEM observations and proof-read the manuscript; W.B. and N.L. discussed the experiments and the manuscript. All authors have read and agreed to the published version of the manuscript.

**Funding:** This research was funded by the Thailand Science Research and Innovation (TSRI), grant number RE-KRIS/008/64.

**Institutional Review Board Statement:** Not applicable.

**Informed Consent Statement:** Not applicable.

**Data Availability Statement:** The data presented in this study are available on request from the corresponding author.

**Acknowledgments:** The authors would like to thank the Scientific Instruments Center KMITL for supporting TGA, FTIR, XRD, and SEM techniques.

**Conflicts of Interest:** The authors declare no conflict of interest.

## References

1. Yang, H.; Yan, N. Transformation of Seafood Wastes into Chemicals and Materials. *Encycl. Sustain. Sci. Technol.* **2018**. [CrossRef]
2. FAO. *The State of World Fisheries and Aquaculture 2020. Sustainability in Action*; FAO: Rome, Italy, 2020.
3. Yan, N.; Chen, X. Sustainability: Don't waste seafood waste. *Nature* **2015**, *524*, 155–157. [CrossRef] [PubMed]
4. Miculescu, F.; Mocanu, A.-C.; Maidaniuc, A.; Dascălu, C.-A.; Miculescu, M.; Voicu, Ș.I.; Ciocoiu, R.-C. Biomimetic Calcium Phosphates Derived from Marine and Land Bioresources. *Hydroxyapatite Adv. Compos. Nanomater. Biomed. Appl. Its Technol. Facet.* **2017**. [CrossRef]
5. Vecchio, K.S.; Zhang, X.; Massie, J.B.; Wang, M.; Kim, C.W. Conversion of bulk seashells to biocompatible hydroxyapatite for bone implants. *Acta Biomater.* **2007**, *3*, 910–918. [CrossRef]
6. Zhang, X.; Vecchio, K.S. Conversion of natural marine skeletons as scaffolds for bone tissue engineering. *Front. Mater. Sci.* **2013**, *7*, 103–117. [CrossRef]
7. Wu, S.-C.; Hsu, H.-C.; Wu, Y.-N.; Ho, W.-F. Hydroxyapatite synthesized from oyster shell powders by ball milling and heat treatment. *Mater. Charact.* **2011**, *62*, 1180–1187. [CrossRef]
8. Shavandi, A.; Bekhit, A.E.-D.A.; Ali, A.; Sun, Z. Synthesis of nano-hydroxyapatite (nHA) from waste mussel shells using a rapid microwave method. *Mater. Chem. Phys.* **2015**, *149–150*, 607–616. [CrossRef]
9. Bhattacharjee, B.N.; Mishra, V.K.; Rai, S.B.; Parkash, O.; Kumar, D. Structure of apatite nanoparticles derived from marine animal (crab) shells: An environment-friendly and cost-effective novel approach to recycle seafood waste. *ACS Omega* **2019**, *4*, 12753–12758. [CrossRef] [PubMed]
10. Ferraz, E.; Gamelas, J.A.F.; Coroado, J.; Monteiro, C.; Rocha, F. Recycling waste seashells to produce calcitic lime: Characterization and wet slaking reactivity. *Waste Biomass Valor.* **2019**, *10*, 2397–2414. [CrossRef]
11. Dampang, S.; Purwanti, E.; Destyorini, F.; Kurniawan, S.B.K.B.; Abdullah, S.R.S.; Imron, M.F. Analysis of optimum temperature and calcination time in the production of CaO using seashells waste as $CaCO_3$ source. *J. Ecol. Eng.* **2021**, *22*, 221–228. [CrossRef]
12. Janković, B.; Smičiklas, I.; Manić, N.; Mraković, A.; Mandić, M.; Veljović, Đ.; Jović, M. Thermo-oxidative evolution and physico-chemical characterization of seashell waste for application in commercial sectors. *Thermochim. Acta* **2020**, *686*, 178568. [CrossRef]
13. Li, Y.; Huang, P.; Guo, S.; Nie, M. A promising and green strategy for recycling waste oyster shell powder as bio-filler in polypropylene via mycelium-enlightened interfacial interlocking. *J. Clean. Prod.* **2020**, *272*, 122694. [CrossRef]

14. Peksen, C.; Koroglu, L.; Kartal, H. Utilization of seashells in matte glaze preparation. *Int. J. Appl. Ceram. Technol.* **2020**, *17*, 1940–1947. [CrossRef]
15. Her, S.; Park, T.; Zalnezhad, E.; Bae, S. Synthesis and characterization of cement clinker using recycled pulverized oyster and scallop shell as limestone substitutes. *J. Clean. Prod.* **2021**, *278*, 123987. [CrossRef]
16. Wang, J.; Liu, E. Upcycling waste seashells with cement: Rheology and early-age properties of Portland cement paste. *Resour. Conserv. Recycl.* **2020**, *155*, 104680. [CrossRef]
17. Seo, J.H.; Park, S.M.; Yang, B.J.; Jang, J.G. Calcined oyster shell powder as an expansive additive in cement mortar. *Materials* **2019**, *12*, 1322. [CrossRef]
18. Wang, Q.; Jiang, F.; Ouyang, X.-K.; Yang, L.-Y.; Wang, Y. Adsorption of Pb(II) from aqueous solution by mussel shell-based adsorbent: Preparation, characterization, and adsorption performance. *Materials* **2021**, *14*, 741. [CrossRef] [PubMed]
19. Larraguibel, A.; Navarrete-Calvo, A.; García, S.; Armijos, V.F.; Caraballo, M.A. Exploring sulfate and metals removal from Andean acid mine drainage using $CaCO_3$-rich residues from agri-food industries and witherite ($BaCO_3$). *J. Clean. Prod.* **2020**, *274*, 123450. [CrossRef]
20. Magnabosco, G.; Giuri, D.; Di Bisceglie, A.P.; Scarpino, F.; Fermani, S.; Tomasini, C.; Falini, G. New material perspective for waste seashells by covalent functionalization. *ACS Sustain. Chem. Eng.* **2021**, *9*, 6203–6208. [CrossRef]
21. Wei, D.; Zhang, H.; Cai, L.; Guo, J.; Wang, Y.; Ji, L.; Song, W. Calcined mussel shell powder (CMSP) via modification with surfactants: Application for antistatic oil-removal. *Materials* **2018**, *11*, 1410. [CrossRef]
22. FAO. *The State of World Fisheries and Aquaculture 2018-Meeting the Sustainable Development Goals*; FAO: Rome, Italy, 2018.
23. Jovic, M.; Mandic, M.; Sljivic-Ivanovic, M.; Smiciklas, I. Recent trends in application of shell waste from mariculture. *Stud. Mar.* **2019**, *32*, 47–62.
24. Seesanong, S.; Laosinwattana, C.; Chaiseeda, K.; Boonchom, B. A simple and rapid transformation of golden apple snail (*Pomacea canaliculata*) shells to calcium carbonate, monocalcium and tricalcium phosphates. *Asian J. Chem.* **2019**, *31*, 2522–2526. [CrossRef]
25. Seesanong, S.; Laosinwattana, C.; Boonchom, B. Microparticles of calcium carbonate $CaCO_3$, calcium hydrogen phosphate hydrate $CaHPO_4 \cdot 1.9H_2O$ and tricalcium phosphate $Ca_3(PO_4)_2$ prepared from golden apple snail shells (*Pomacea canaliculata*). *Res. J. Chem. Environ.* **2020**, *24*, 1–6.
26. Sánchez-Enríquez, J.; Reyes-Gasga, J. Obtaining $Ca(H_2PO_4)_2 \cdot H_2O$, monocalcium phosphate monohydrate, via monetite from brushite by using sonication. *Ultrason. Sonochem.* **2013**, *20*, 948–954. [CrossRef]
27. Dorozhkin, S.V. Biphasic, Triphasic, and Multiphasic Calcium Orthophosphates. In *Advanced Ceramic Materials*; Tiwari, A., Gerhardt, R.A., Szutkowska, M., Eds.; Scrivener Publishing: Beverly, MA, USA, 2016; pp. 33–95.
28. Hsu, Y.-S.; Chang, E.; Liu, H.-S. Hydrothermally-grown monetite ($CaHPO_4$) on hydroxyapatite. *Ceram. Int.* **1998**, *24*, 249–254. [CrossRef]
29. Gonzalez-McQuire, R.; Chane-Ching, J.-Y.; Vignaud, E.; Lebugle, A.; Mann, S. Synthesis and characterization of amino acid-functionalized hydroxyapatite nanorods. *J. Mater. Chem.* **2004**, *14*, 2277–2281. [CrossRef]
30. Liu, J.; Li, K.; Wang, H.; Zhu, M.; Yan, H. Rapid formation of hydroxyapatite nanostructures by microwave irradiation. *Chem. Phys. Lett.* **2004**, *396*, 429–432. [CrossRef]
31. Kong, X.-D.; Sun, X.-D.; Lu, J.-B.; Cui, F.-Z. Mineralization of calcium phosphate in reverse microemulsion. *Curr. Appl. Phys.* **2005**, *5*, 519–521. [CrossRef]
32. Boonchom, B.; Danvirutai, C. The morphology and thermal behavior of calcium dihydrogen phosphate monohydrate ($Ca(H_2PO_4)_2 \cdot H_2O$) obtained by a rapid precipitation route at ambient temperature in different media. *J. Optoelectron. Biomed. Mater.* **2009**, *1*, 115–123.
33. Liu, D.-M.; Yang, Q.; Troczynski, T.; Tseng, W.J. Structural evolution of sol–gel-derived hydroxyapatite. *Biomaterials* **2002**, *23*, 1679–1687. [CrossRef]
34. Sivakumar, G.R.; Girija, E.K.; Narayana Kalkura, S.; Subramanian, C. Crystallization and characterization of calcium phosphates: Brushite and monetite. *Cryst. Res. Technol.* **1998**, *33*, 197–205. [CrossRef]
35. Rohanizadeh, R.; LeGeros, R.Z.; Harsono, M.; Bendavid, A. Adherent apatite coating on titanium substrate using chemical deposition. *J. Biomed. Mater. Res. A* **2005**, *72*, 428–438. [CrossRef] [PubMed]
36. Djošić, M.S.; Mišković-Stanković, V.B.; Kačarević-Popović, Z.M.; Jokić, B.M.; Bibić, N.; Mitrić, M.; Milonjić, S.K.; Jančić-Heinemann, R.; Stojanović, J. Electrochemical synthesis of nanosized monetite powder and its electrophoretic deposition on titanium. *Colloids Surf. A Physicochem. Eng. Asp.* **2009**, *341*, 110–117. [CrossRef]
37. Suchanek, W.L.; Shuk, P.; Byrappa, K.; Riman, R.E.; TenHuisen, K.S.; Janas, V.F. Mechanochemical–hydrothermal synthesis of carbonated apatite powders at room temperature. *Biomaterials* **2002**, *23*, 699–710. [CrossRef]
38. Onoda, H.; Nakanishi, H. Preparation of calcium phosphate with oyster shells. *Nat. Resour.* **2012**, *3*, 71–74. [CrossRef]
39. Macha, I.J.; Ozyegin, L.S.; Chou, J.; Samur, R.; Oktar, F.N.; Ben-Nissan, B. An alternative synthesis method for di calcium phosphate (monetite) powders from Mediterranean mussel (*Mytilus galloprovincialis*) shells. *J. Aust. Ceram. Soc.* **2013**, *49*, 122–128.
40. Karunadasa, K.S.P.; Manoratne, C.H.; Pitawala, H.M.T.G.A.; Rajapakse, R.M.G. Thermal decomposition of calcium carbonate (calcite polymorph) as examined by in-situ high-temperature X-ray powder diffraction. *J. Phys. Chem. Solids* **2019**, *134*, 21–28. [CrossRef]
41. Seesanong, S.; Laosinwattana, C.; Boonchom, B. A simple rapid route to synthesize monocalcium phosphate monohydrate using calcium carbonate with different phases derived from green mussel shells. *J. Mater. Environ. Sci.* **2019**, *10*, 113–118.

42. Nakamoto, K. *Infrared and Raman Spectra of Inorganic and Coordination Compounds: Part A: Theory and Applications in Inorganic Chemistry*, 6th ed.; John Wiley & Sons: Hoboken, NJ, USA, 2008.
43. Cotton, F.A. *Chemical Applications of Group Theory*, 3rd ed.; Wiley-Interscience: New York, NY, USA, 1990.
44. Koura, N.; Kohara, S.; Takeuchi, K.; Takahashi, S.; Curtiss, L.A.; Grimsditch, M.; Saboungi, M.-L. Alkali carbonates: Raman spectroscopy, ab initio calculations, and structure. *J. Mol. Struct.* **1996**, *382*, 163–169. [CrossRef]
45. Rahman, M.A.; Oomori, T. Structure, crystallization and mineral composition of sclerites in the alcyonarian coral. *J. Cryst. Growth* **2008**, *310*, 3528–3534. [CrossRef]
46. Boonchom, B. Parallelogram-like microparticles of calcium dihydrogen phosphate monohydrate ($Ca(H_2PO_4)_2 \cdot H_2O$) obtained by a rapid precipitation route in aqueous and acetone media. *J. Alloys Compd.* **2009**, *482*, 199–202. [CrossRef]
47. Koleva, V.; Stefov, V.; Najdoski, M.; Cahil, A. Vibrational spectra of cobalt dihydrogen phosphate dihydrate, $Co(H_2PO_4)_2 \cdot 2H_2O$. *Vib. Spectrosc.* **2012**, *62*, 229–237. [CrossRef]
48. Koleva, V.; Stefov, V. Phosphate ion vibrations in dihydrogen phosphate salts of the type $M(H_2PO_4)_2 \cdot 2H_2O$ (M=Mg, Mn, Co, Ni, Zn, Cd): Spectra–structure correlations. *Vib. Spectrosc.* **2013**, *64*, 89–100. [CrossRef]
49. Xu, J.; Gilson, D.F.R.; Butler, I.S. FT-Raman and high-pressure FT-infrared spectroscopic investigation of monocalcium phosphate monohydrate, $Ca(H_2PO_4)_2 \cdot H_2O$. *Spectrochim. Acta A* **1998**, *54*, 1869–1878. [CrossRef]
50. Rangavittal, N.; Landa-Cánovas, A.R.; González-Calbet, J.M.; Vallet-Regí, M. Structural study and stability of hydroxyapatite and β-tricalcium phosphate: Two important bioceramics. *J. Biomed. Mater. Res.* **2000**, *51*, 660–668. [CrossRef]
51. Prevéy, P.S. X-ray diffraction characterization of crystallinity and phase composition in plasma-sprayed hydroxyapatite coatings. *J. Therm. Spray Technol.* **2000**, *9*, 369–376. [CrossRef]